Volume 1 | Number 1 | Jan 2013 | Pages 1–100

Journal of
Materials Chemistry A

Materials for energy and sustainability
www.rsc.org/materialsA

Li⁺

ROYAL SOCIETY
OF CHEMISTRY

ROYAL SOCIETY
OF CHEMISTRY

www.rsc.org/materialsA

Table of Contents entry

A simple and low-cost method for the preparation of self-supported TiO$_2$:WO$_3$ ceramic heterojunction wafers

Neel M. Makwana[a], Raul Quesada-Cabrera[a], Ivan P. Parkin[a], Paul F. McMillan[a], Andrew Mills[b] and Jawwad A. Darr*[a]
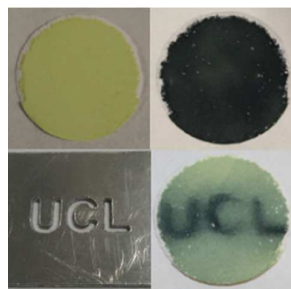
Self-supported ceramic heterojunction wafers prepared by a simple, low-cost method, show efficient vectorial charge separation and increased photocatalytic rates.

Journal of Materials Chemistry A

A simple and low-cost method for the preparation of self-supported TiO₂:WO₃ ceramic heterojunction wafers

Neel M. Makwana[a], Raul Quesada-Cabrera[a], Ivan P. Parkin[a], Paul F. McMillan[a], Andrew Mills[b] and Jawwad A. Darr*[a]

Robust, bilayer heterojunction photodiodes of TiO₂:WO₃ were prepared successfully by a simple, low-cost powder pressing technique followed by heat-treatment. Exclusive photoirradiation of the TiO₂ side of the photodiode resulted in a rapid colour change (dark blue) on the WO₃ surface as a result of reduction of W^{6+} to W^{5+} (confirmed by X-ray photoelectron spectroscopy). This colour was long lived and shown to be stable in a dry environment in air for several hours. A similar photoirradiation experiment in the presence of a mask showed that charge transfer across the heterojunction occurred approximately normal to the TiO₂ surface, with little smearing out of the mask image. As a result of the highly efficient vectorial charge separation, the photodiodes showed a tremendous increase in photocatalytic activity for the degradation of stearic acid, compared to wafers of the respective individual materials when tested separately.

Introduction

Solar energy harvesting devices including heterojunction solar cells and semiconductor photocatalysts effectively harness part of the Sun's energy via efficient formation and separation of photogenerated excitons.[1-6] Earlier reports in the literature focused on selecting and tuning semiconductors (e.g. by addition of dopant atoms[7,8]) with appropriate band gaps for light absorption, and selecting band edge positions relevant to the targeted reduction and oxidation processes. However, for a single material, it is difficult to combine the desired characteristics of efficient light absorption in the required wavelength range while matching the redox potentials, and minimizing recombination and trapping processes. Recently, researchers in the field have begun to develop photoelectrochemical devices consisting of two or more coupled semiconductor materials as thin films or particles using materials with complementary band edge positions that make it easier to design and control elements of the light absorption, redox and charge separation processes. These arrangements substantially reduce the occurrence of the back reaction (i.e. electron – hole recombination).[9-12] Architectural design of such solar driven devices based on coupled semiconductor systems, is thus critical for developing high solar efficiencies.

In a heterojunction photocatalytic system, photogenerated electrons and holes at different sides of the junction participate in a variety of surface oxidation reactions, including organic pollutant degradation,[13-16] oxidation of water to O₂,[17] or the removal of harmful bacteria or organisms,[18,19] that are typically coupled with the concomitant reduction of oxygen to water at the opposing (often dark) junction. Because of efficient vectorial charge separation, heterojunction photocatalysts or devices can display superior performance compared to analogous single semiconductor systems.[20]

It is important to develop efficient, reliable and cost-effective methods to produce such coupled photoelectrochemically active systems. Heterojunction photocatalytic materials consisting of multiple layered or composite semiconductors, or on different crystal facets[21] have been prepared using a range of synthesis methods, some of which can be laborious, often involving multiple steps (e.g. ion-exchange precipitation reactions[17,22,23]) and taking many hours to complete, or requiring expensive and specialized equipment or precursors (such as chemical vapour deposition,[16] sol-gel synthesis,[14,24] and batch hydrothermal synthesis[25-27]). Often, in the case of layered heterojunction photocatalytic materials, a substrate layer is required upon which the heterojunction is deposited/fabricated, and although it may not take part in the photocatalytic reaction, it can be considered an additional cost in the process. Therefore, simpler, inexpensive synthesis routes based on readily available and sustainable precursors and elements to form robust, self-

This journal is © The Royal Society of Chemistry 2014

J. Mater. Chem. A, 2014, **00**, 1-3 | **1**

supported, semiconductor heterojunction photocatalytic systems, are desirable.

Recently, the authors reported a simple and inexpensive method of producing self-supporting wafers of photocatalytically active TiO_2 powders, using a cold-pressing technique.[28] Here we have extended the simple method to prepare self-supported photocatalytic heterojunction (SPH) photodiodes using commercially available WO_3 and TiO_2 powders. The resulting photodiodes incorporate a relatively stable charge-transfer heterojunction between the TiO_2 and WO_3 layers and show enhanced photocatalytic performance for the degradation of stearic acid, a well-known organic pollutant, compared to wafers of the individual photocatalysts.

Experimental

Chemicals and materials

Industrial grade titanium dioxide PC50 (anatase) was obtained from Cristal Global (Stallingborough, UK) and tungsten(VI) oxide (99.8% metals basis) was obtained from Alfa Aesar (Lancashire, UK). Stearic acid (reagent grade, 95%) was obtained from Sigma-Aldrich (Dorset, UK).

Preparation of TiO_2/WO_3 ceramic photodiodes

Ceramic photodiodes were prepared by pressing powders in a circular 25 mm diameter stainless steel die (Compacting Tooling Inc., Philadelphia, USA) at a pressure of 200 bar in the extraction ram of a non-end-loaded piston cylinder press[29] (Depths of the Earth Company, Arizona, USA) following a similar procedure to Elouali et al.[28] It was found that an even powder distribution was important for the preparation of thin and robust wafers. To prevent the powder from sticking to the die, Mylar® sheets cut to size were placed on each die surface and a razor blade was used to level the powder surface. This aided in achieving a uniform thickness while minimizing wafer fracture. For the preparation of the layered wafers (illustrated in Fig. S1), TiO_2 (0.3 g) was first placed in the die and leveled to create an even surface, followed by the addition of WO_3 (0.7 g) on top of the TiO_2 layer. After pressing, the ceramic photodiodes were heat-treated in air at 500 °C for 6 h to enhance wafer robustness. As shown in Fig. 3a some cracking occurred at the edges of the WO_3 layer; however, the bulk of the wafers remained intact throughout testing and handling.

Investigation of heterojunction charge-transfer

In a typical experiment, the ceramic wafer was placed in a sacrificial solution consisting of 1:1 $EtOH$:H_2O containing 0.1 M HCl. The TiO_2 surface was irradiated with simulated solar light using a 75W xenon light source (Photon Technology International, West Sussex, UK) fitted with an AM 1.5G filter (Newport Spectra-Physics Ltd., Oxfordshire, UK; spectral output shown in Fig. S3a) with lamp to sample distance of 14 cm. In experiments to determine the directionality of electron

transfer pathways, a region of the TiO_2 surface of the ceramic wafer was masked for selective photoirradiation of the surface. A template prepared from a 1 mm sheet of aluminum via CNC milling was cut-out with the lettering 'UCL' (Fig. S2) to investigate the electron transport pathways through the ceramic wafer. The template was placed directly on the TiO_2 surface of the ceramic wafer and photoirradiation was carried out exactly as mentioned earlier.

Stearic acid (SA) photocatalytic degradation tests

The photocatalytic performance of each pressed wafer was determined by the photocatalytic degradation of SA by the amount of evolved CO_2 monitored by FTIR spectroscopy at regular intervals. Stearic acid (50 μL (10 μL for sample A2b), 0.05 M in $CHCl_3$) was placed on the centre of the wafer surface of interest, and the solvent allowed to evaporate. The coated wafer was placed in a gastight glass cell fitted with KBr windows and the internal atmosphere of the cell purged with argon gas to remove traces of CO_2. The wafer was placed with the irradiated surface (as indicated in Fig. 5a-c) facing upwards so that the surface was under direct UVA irradiation from 2 × 8W 365 nm UV lamp (Uvitec, Cambridge, UK; spectral output shown in Fig. S3b). The IR spectrum through the gas cell was measured at regular intervals (PerkinElmer Spectrum RXI with Spectrum v5.3.1 software). To ensure no contamination from atmospheric CO_2, the sample chamber in the IR instrument (within which the gas cell was placed for measurement) was purged with argon gas for 5 minutes prior to each measurement. A series of control experiments were carried out under irradiation; (i) an empty gas cell, (ii) a TiO_2 wafer in the absence of stearic acid, and (iii) stearic acid on a glass substrate, to confirm the presence of atmospheric CO_2 did not interfere with the measurements.

Ceramic wafer characterisation

X-ray diffraction (XRD) data was collected using a Stoe Stadi P diffractometer (Mo-Kα radiation, 0.70932 Å) in transmission geometry (2 - 40° 2θ range, 0.5° step size and 5 sec/step dwell). X-ray photoelectron spectroscopy (XPS) measurements were collected using a Thermo Scientific™ K-Alpha™+ spectrometer using Al-Kα radiation with a constant pass energy of 50 eV. Data was analysed using CasaXPS™ software (version 2.3.16). Field emission scanning electron microscopy (FE-SEM) images were obtained with a JEOL JSM-6700F microscope operating at 5 kV accelerating voltage. As-prepared ceramic wafers were cracked to expose the cross-sectional interface between the TiO_2 and WO_3 layers, and all samples were gold coated prior to imaging. Image analysis was performed using ImageJ software (version 1.48v).

Results and discussion

Investigation of heterojunction charge-transfer

2 | J. Mater. Chem. A, 2014, 00, 1-3

This journal is © The Royal Society of Chemistry 2014

When a TiO_2:WO_3 SPH monolith was placed in a sacrificial electron donor solution and photoirradiated on the TiO_2 side only, a significant, gradual dark blue colouration of the non-illuminated, i.e. 'dark', WO_3 side was observed within 45 minutes. Consideration of the expected conduction and valence band positions of TiO_2 and WO_3 (Fig. 1) would lead to the conclusion that in the SPH monoliths, photogenerated electrons in the conduction band (CB) of TiO_2 would be shuttled across the heterojunction and into the CB of WO_3, whereas the photogenerated holes would react irreversibly with the sacrificial electron donor, ethanol. Therefore, the electrons would be expected to accumulate in the conduction band of WO_3 where W^{6+} in the WO_3 crystal lattice could be reduced to W^{5+}, causing a dark blue colouration that intensifys with increasing irradiation time. Indeed, as the photoirradiated wafers retained their colour for several hours when dried, it was possible to confirm, by X-ray photoelectron spectroscopy (XPS), the presence of W^{5+} species as being responsible for the colour change (Fig. 2). The two major $4f_{7/2}$ and $4f_{5/2}$ peaks centred at 35.61 and 37.79 eV are assigned to W^{6+} and the two smaller $4f_{7/2}$ and $4f_{5/2}$ peaks centred at 34.45 and 36.59 eV are assigned to W^{5+}. The reoxidation of W^{5+} to W^{6+} by oxygen in air was very slow with the original, yellow/green colour of the WO_3 only fully reappearing after approximately 1 week following photo-activation, i.e. "charging". This suggests the SPH's could have potential applications as light-activated oxygen indicators or reusable writing media.

Following the onset of irradiation at the TiO_2 side, the first observation of the light induced colour change at the WO_3 surface occurred within 2 minutes. Over a period of 45 minutes the WO_3 surface changed rapidly from light green to dark blue (Fig. 3a and b). When the test was repeated with direct irradiation of the WO_3 surface a colour change was only observed at the edge of the wafer where some TiO_2 was exposed due to a small amount of flaking of the WO_3 layer (Fig. 3a; the flaking occurred as a result of the large micron size WO_3 powder having poor granular adhesion and non-optimised pressing procedure). This confirms that the electrons responsible for the colour change were photogenerated in the TiO_2, transported across the heterojunction and accumulated in the WO_3 CB, where they reduced W^{6+} to W^{5+}. In both cases with irradiation of either the TiO_2 or WO_3 side, the TiO_2 surface always remained white. When the wafer was irradiated with visible light only (obtained by placing a UV 420 nm cut-off filter, Optivex™, between the lamp and sample) no colour change in the WO_3 side was observed, suggesting that the effect could only be produced via UV irradiation of the TiO_2. Although it might be expected that visible light irradiation of the WO_3 surface should result in appearance of a blue colour due to the reduction of W^{6+} to W^{5+}, this process appeared to be very slow, implying the trapping of the photogenerated holes on the WO_3 by the ethanol was much less effective than it was for TiO_2, and a colour change on the WO_3 was not observed on the timescale of this irradiation (*ca.* 1 hour) performed herein. While thin films of TiO_2:WO_3 are known for photocatalytic and photochromic applications,[30-33] the interaction between each

semiconductor is often gained through layered growth to form good electronic contact between the materials. In contrast, here, a stable interface with excellent electronic contact is formed between the TiO_2 and WO_3 powders solely through the application of high-pressure pressing (the heat treatment is used only to strengthen the wafers and studies have shown the electronic contact is present even before heat-treatment).

To demonstrate the directionality of electron transfer through the bilayer ceramic wafer, an aluminium mask with the letters 'UCL' cut-out (Fig. S2) was placed on the TiO_2 side to partially block the light irradiation (Fig. 3c). Rapid darkening of the WO_3 side was observed with the 'UCL' lettering from the mask appearing with little distortion (Fig. 3d and e). This observation indicated that charge transfer across the heterojunction and through the wafer occurred approximately normal to the illuminated TiO_2 surface with little spreading. This could indicate that the carrier mean path followed a line of least resistance between the photoactivated sites and the WO_3/air interface. This would be considered beneficial to photocatalytic applications because shorter electron transfer pathways lead to more efficient overall photocatalytic processes.[4,34]

Stearic acid degradation experiments

To assess the photocatalytic activity of a self-supported TiO_2:WO_3 SPH compared to an individual single powder monolith pressed ceramic wafer, we employed a stearic acid (SA) degradation test under UVA (365 nm) irradiation. Stearic acid is used as a typical model compound for the hydrophobic, wax-like organic pollutants that may coat internal and external surfaces. The degradation of stearic acid is a mineralization process[35] which proceeds to form carbon dioxide and water, as shown in equation (1):

$$CH_3(CH_2)_{16}CO_2H + 26O_2 \xrightarrow{semiconductor; h\nu \geq E_{bg}} 18CO_2 + 18H_2O \quad (1)$$
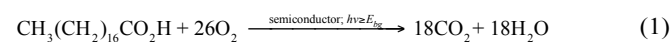
This process can be followed using FTIR spectroscopy to monitor the disappearance of stearic acid. However, the technique is not practical for studying the pressed powder wafers used here. Therefore, as a method of assessing the efficacy of reaction (1), we chose to monitor by FTIR the amount of CO_2 released into the gas phase.

A TiO_2:WO_3 SPH monolith coated on one side with SA was placed inside a gastight IR glass cell and illuminated with UVA light (365 nm; UV irradiance at the sample surface was *ca.* 0.59 mW/cm^2). The FTIR spectrum of the headspace above the sample was measured at regular intervals in order to follow the increase in evolved CO_2. Fig. 4 shows a typical set of IR absorbance spectra obtained, in which there is the emergence of peaks in the range 2250-2400 cm^{-1}, which correspond to the asymmetric and symmetric stretching modes of CO_2.[35] The integrated area under the CO_2 absorbance peak for each IR spectrum, which is proportional to the concentration of CO_2 in the gas phase, was plotted as a function of irradiation time (Fig. 5d). Control experiments carried out in the absence of a photocatalyst and UVA light confirmed that CO_2 detected

within the gas cell was evolved through the photocatalysed degradation process.

Fig. 5a-c identifies which surface of the TiO_2:WO_3 SPH monolith was coated with stearic acid and which surface was illuminated. Also shown are the expected electron-hole transfer pathways (e⁻ and h⁺ with arrows) in each irradiation scenario. Sample A2 (TiO_2:WO_3 SPH monolith with SA on the TiO_2 side) exhibited a rate of CO_2 generation eight times that of a TiO_2 only ceramic wafer (sample A1). For samples A1 and A2, the photogenerated holes are able to effect, either by direct or an indirect electron transfer mechanism, the oxidative degradation of SA. The lower CO_2 evolution rate of sample A1 may be attributed to a less efficient vectorial separation of the photogenerated electrons and holes and so a greater rate of electron-hole recombination occurring within the pure TiO_2 wafer and on its surface. Conducting the degradation experiment with smaller amounts of SA showed that the degradation rate was independent of the quantity of SA present, as shown for sample A2b (a TiO_2:WO_3 SPH monolith with 10 μL of 0.05 M SA in $CHCl_3$ solution on the TiO_2 side). Sample A3 (SPH with SA on WO_3 side and irradiation on the TiO_2) appeared slightly more effective than sample A1 for SA degradation. Kim et al. have shown that WO_3, when photoexcited, can generate hydroxyl radicals via reductive decomposition of H_2O_2 that is produced by reduction of O_2 on WO_3.[36] Thus, it is also likely herein that photogenerated electrons on the surface of WO_3 generate H_2O_2, which can act as a secondary source of hydroxyl radicals that are effective in aiding photocatalytic SA oxidation. The photogenerated holes would then be able to oxidize surface adsorbed H_2O to O_2. In contrast, a TiO_2:WO_3 SPH with SA and UVA light on the WO_3 surface yielded very little CO_2.

The data presented in Fig 5(d) can be used to determine the initial formal quantum efficiency (FQE) for the removal of SA, defined as the ratio between the SA molecule degradation rate and incident photon flux. The photon flux for the UVA light source was calculated as 1.09×10^{15} photons cm⁻² s⁻¹. The average values of the FQE and SA degradation rate are provided in Table 1. From the FQE values reported, it is clear that the photocatalytic activity is higher for the TiO_2:WO_3 heterojunction wafers, and similar findings are reported in the literature for composite thin films of TiO_2:WO_3.[16]

Ceramic wafer characterisation

The ceramic wafers were analysed by XRD before and after heat treatment. An XRD pattern of the TiO_2 phase (Fig. 6) confirms the TiO_2 remains in the anatase structure. FE-SEM images are shown in Fig. 7 where the distinction between the TiO_2 and WO_3 layers is clearly apparent; suggesting the interaction between the layers is a physical, rather than chemical, interaction. Also apparent from the image is the large difference in particle size between the two materials (Fig. 7(a)-(b)). Despite this difference, the results described in this work demonstrated that electron transfer is still feasible between the particles. The average thickness of the WO_3 layer was

measured as 82.2 ± 3.2 μm. Fig. 7(c) shows an image of the WO_3 layer where loosely bound particles are seen in the area marked *a*. Upon cracking of the ceramic wafer (to enable imaging across the heterojunction interface) the physical interaction between particles may have disrupted, resulting in loosened particles. Conversely, the area marked *b* shows particles in very close contact in the horizontal plane (which is also the direction of compaction), across which it is believed charge transport occurs. Fig. 7(d) shows an image of the TiO_2 layer, although analysis was limited due to the low resolution of the image.

Conclusions

In closing, the findings presented herein show that simple and robust TiO_2:WO_3 SPH monoliths can be manufactured using a low-cost method by pressing the relevant powder assemblies together at high pressure, followed by heat treatment to increase strength. The wafers are self-supported and thus do not require a support layer. While TiO_2 is known to be an efficient photocatalyst in its own right, the formation of a semiconductor heterojunction material with WO_3 provides greater control over and enhances its photocatalytic activity. One main factor leading to this is the vectorial charge separation and reduction in electron-hole recombination due to the efficient transfer of photogenerated electrons between the TiO_2 and WO_3 layers. The findings demonstrate that an intimate electronic contact can be developed between different photocatalytic powders through high-pressure pressing only, not requiring multiple, often complex, reaction steps or taking many hours to complete.

To our knowledge, this is the first report of a self-supported, bilayer heterojunction prepared by a simple technique, for which there is considerable potential for improved photocatalytic performance and applications. By carefully selecting appropriate photocatalyst combinations to best exploit band gaps and relative band positions (under suitable conditions), it should be possible in the future to facilitate heterojunctions for a wide range of photocatalytic reactions, such as water splitting and CO_2 reduction.

Acknowledgements

Notes and references

a Christopher Ingold Laboratories, Department of Chemistry, University College London, 20 Gordon Street, London, WC1H 0AJ, United Kingdom. E-mail: j.a.darr@ucl.ac.uk
b School of Chemistry and Chemical Engineering, Queen's University Belfast, Stranmillis Road, Belfast, BT9 5AG, United Kingdom

1. A. Fujishima and K. Honda, *Nature*, 1972, **238**, 37-38.
2. A. J. Heeger, *Adv. Mater.*, 2013, **26**, 10-28.
3. R. Pandey and R. J. Holmes, *Adv. Mater.*, 2010, **22**, 5301-5305.
4. A. Kudo and Y. Miseki, *Chem. Soc. Rev.*, 2008, **38**, 253.
5. A. J. Cowan and J. R. Durrant, *Chem. Soc. Rev.*, 2013, **42**, 2281.
6. R. Abe, *J. Photochem. Photobiol., C*, 2010, **11**, 179-209.
7. R. Asahi, *Science*, 2001, **293**, 269-271.
8. A. Zaleska, *Recent Pat. Eng.*, 2008, **2**, 157-164.
9. K. Maeda, *ACS Catal.*, 2013, **3**, 1486-1503.
10. S. B. Rawal, S. Bera, D. Lee, D.-J. Jang and W. I. Lee, *Catal. Sci. Technol.*, 2013, **3**, 1822.
11. A. Kubacka, M. Fernández-García and G. Colón, *Chem. Rev.*, 2012, **112**, 1555-1614.
12. Y. Wang, Q. Wang, X. Zhan, F. Wang, M. Safdar and J. He, *Nanoscale*, 2013, **5**, 8326.
13. Y. R. Do, W. Lee, K. Dwight and A. Wold, *J. Solid State Chem.*, 1994, **108**, 198-201.
14. C. W. Dunnill, S. Noimark and I. P. Parkin, *Thin Solid Films*, 2012, **520**, 5516-5520.
15. Y. Liu, C. Xie, J. Li, T. Zou and D. Zeng, *Appl. Catal., A*, 2012, **433**, 81-87.
16. R. Quesada Cabrera, E. R. Latimer, A. Kafizas, C. S. Blackman, C. J. Carmalt and I. P. Parkin, *J. Photochem. Photobiol., A*, 2012, **239**, 60-64.
17. F. Wang, X. Chen, X. Hu, K. S. Wong and J. C. Yu, *Sep. Purif. Technol.*, 2012, **91**, 67-72.
18. O. Akhavan, *Appl. Surf. Sci.*, 2010, **257**, 1724-1728.
19. O. Akhavan, M. Abdolahad, Y. Abdi and S. Mohajerzadeh, *Carbon*, 2009, **47**, 3280-3287.
20. J. S. Jang, H. G. Kim and J. S. Lee, *Catal. Today*, 2012, **185**, 270-277.
21. J. Yu, J. Low, W. Xiao, P. Zhou and M. Jaroniec, *J. Am. Chem. Soc.*, 2014, **136**, 8839-8842.
22. Y. Bessekhouad, D. Robert and J.-V. Weber, *J. Photochem. Photobiol., A*, 2004, **163**, 569-580.
23. Y. Bessekhouad, D. Robert and J. V. Weber, *Catal. Today*, 2005, **101**, 315-321.
24. D. O. Scanlon, C. W. Dunnill, J. Buckeridge, S. A. Shevlin, A. J. Logsdail, S. M. Woodley, C. R. A. Catlow, M. J. Powell, R. G. Palgrave, I. P. Parkin, G. W. Watson, T. W. Keal, P. Sherwood, A. Walsh and A. A. Sokol, *Nat. Mater.*, 2013, **12**, 798-801.
25. J. Cao, B. Xu, H. Lin and S. Chen, *Chem. Eng. J.*, 2013, **228**, 482-488.
26. H. Huang, S. Wang, N. Tian and Y. Zhang, *RSC Adv.*, 2014, **4**, 5561.
27. H. Zhao, L. Liu, J. M. Andino and Y. Li, *J. Mater. Chem. A*, 2013, **1**, 8209.
28. S. Elouali, A. Mills, I. P. Parkin, E. Bailey, P. F. McMillan and J. A. Darr, *J. Photochem. Photobiol., A*, 2010, **216**, 110-114.
29. E. S. Patera and J. R. Holloway, *Eos Trans. AGU*, 1978, **59**, 1217-1218.
30. Y. Djaoued, S. Balaji and N. Beaudoin, *J. Sol-Gel Sci. Technol.*, 2013, **65**, 374-383.
31. Y. P. He, Z. Y. Wu, L. M. Fu, C. R. Li, Y. M. Miao, L. Cao, H. M. Fan and B. S. Zou, *Chem. Mater.*, 2003, **15**, 4039-4045.
32. T. He, Y. Ma, Y. Cao, X. L. Hu, H. M. Liu, G. J. Zhang, W. S. Yang and J. N. Yao, *J. Phys. Chem. B*, 2002, **106**, 12670-12676.
33. S. Higashimoto, Y. Ushiroda and M. Azuma, *Top. Catal.*, 2008, **47**, 148-154.
34. K. Maeda, *J. Photochem. Photobiol., C*, 2011, **12**, 237-268.
35. A. Mills and J. Wang, *J. Photochem. Photobiol., A*, 2006, **182**, 181-186.
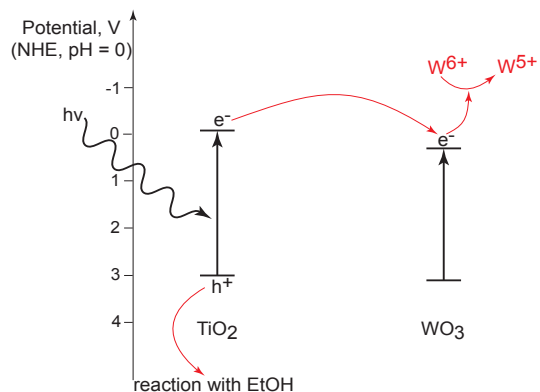36. J. Kim, C. W. Lee and W. Choi, *Environ. Sci. Technol.*, 2010, **44**, 6849-6854.

Fig. 1 Conduction and valence band positions of TiO₂ and WO₃ with arrows showing the proposed mechanism of electron and hole transfer (and subsequent reduction of W^{6+} species).
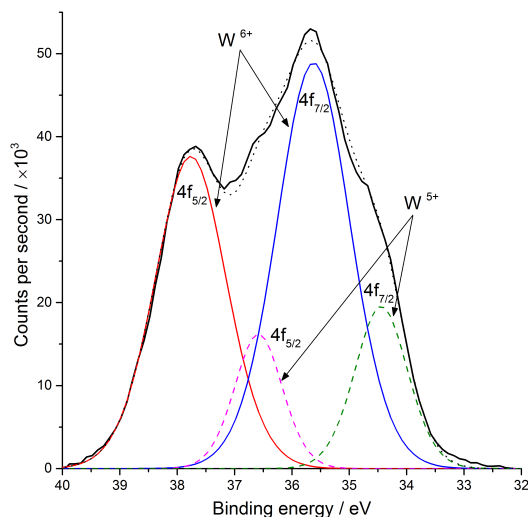

Fig. 2 X-ray photoelectron spectrum showing the presence of W^{5+} reduced states on the WO₃ surface following photoirradiation (75 W xenon lamp) of the TiO₂ surface of a TiO₂:WO₃ self-supported photocatalytic heterojunction.
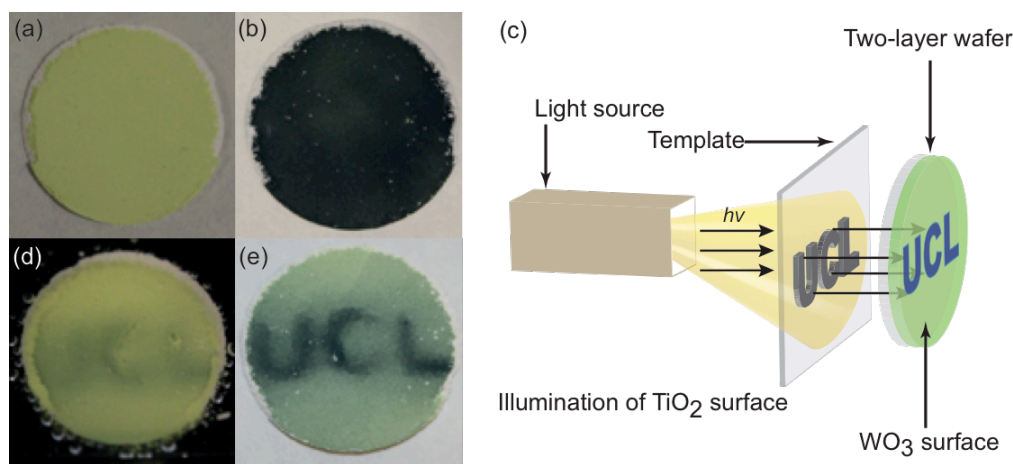

Fig. 3 Image (a) shows the as-prepared TiO₂/WO₃ wafer with the WO₃ surface visible (part of the TiO₂ layer is seen at the edges of the wafer where flaking occurred) and image (b) shows the discoloration of the WO₃ surface after 45 minutes photoirradiation of the TiO₂ surface. (c) Illustration depicting the experimental setup for determining electron transfer pathways using a 'UCL' lettering template. Images (d) and (e) show the appearance of 'UCL' lettering on the WO₃ surface after photoirradiation of the TiO₂ surface using a template at 5 and 35 minutes, respectively. Photoirradiation was from a 75W xenon arc lamp.
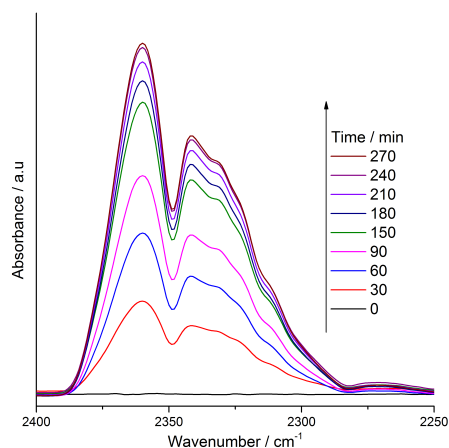
Fig. 4 Typical infrared absorbance spectra obtained for the evolution of CO_2 during the photodegradation of stearic acid on TiO_2/WO_3 wafers under UVA (365 nm) light irradiation.
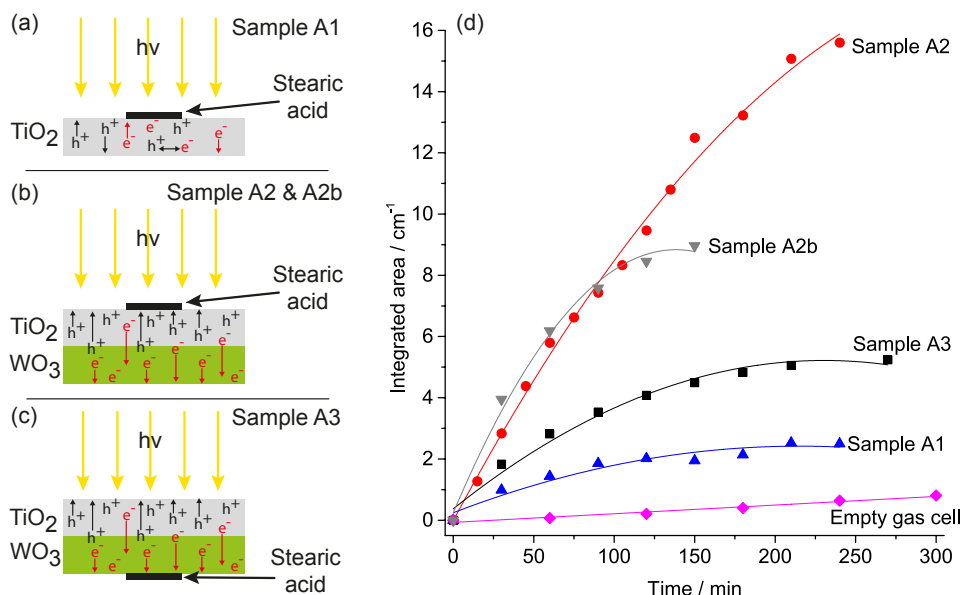

Fig. 5 Schematic diagrams illustrating sample configuration and identifying surface containing stearic acid (SA) and UVA irradiation as: (a) ceramic wafer of TiO_2 only, SA and UVA irradiation on the same surface, (b) self-supported photocatalytic heterojunction (SPH) wafer of TiO_2:WO_3 with SA and UVA irradiation on the TiO_2 surface, and (c) SPH wafer of TiO_2:WO_3 with SA on the WO_3 surface and UVA irradiation on the TiO_2 surface. e^- and h^+ and their corresponding arrows on diagrams (a)-(c) indicate the expected mobility of electrons and holes in the ceramic wafers. (d) shows the CO_2 evolution profile over the course of the degradation of stearic acid on ceramic wafers under UVA irradiation (2 × 8W 365 nm).
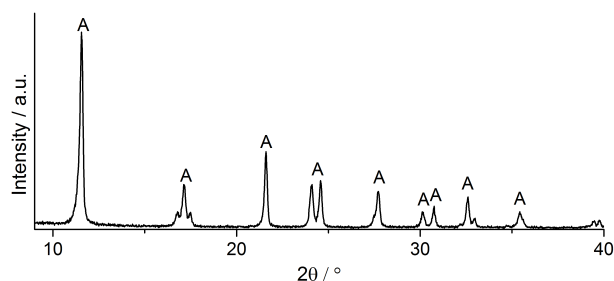

Fig. 6 X-ray diffraction pattern of TiO_2 phase of TiO_2/WO_3 ceramic wafer following heat treatment (500 °C, 6 h) identifying anatase structure.

This journal is © The Royal Society of Chemistry 2014
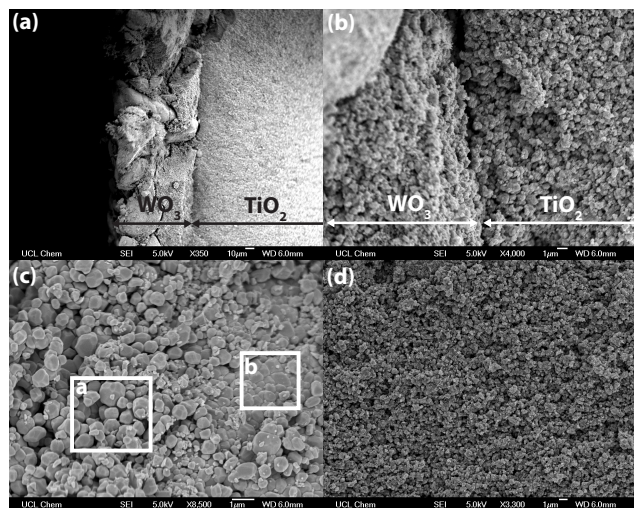
J. Mater. Chem. A, 2014, **00**, 1-3 | **7**

Fig. 7 FE-SEM images of the TiO_2:WO_3 ceramic wafer heterojunction following preparation. Images (a) and (b) show the distinction between the TiO_2 and WO_3 layers and the physical interface between the two materials. Image (c) shows the WO_3 layer, with the area marked *a* showing loosely bound particles as a result of the disrupted physical interaction when the ceramic wafer was cracked for imaging. The area marked *b* shows particles in very close contact, as result of the compaction of the powder upon preparation of the ceramic wafer (the compaction occurred in the horizontal plane). Image (d) shows the TiO_2 layer.

Table 1 Formal quantum efficiency (FQE) and average stearic acid (SA) degradation rate on ceramic wafer samples of TiO_2 and TiO_2:WO_3, as described in Fig. 5.

Sample	FQE $\times10^{-4}$ (molecules photon^{-1})	Rate $\times10^{13}$ (molecules cm^{-2} min^{-1})
A1	1.7	1.1
A2	6.7	4.4
A2b	6.9	4.5
A3	2.7	1.8